Physical properties of Polyakov loop geometrical clusters in SU(2) gluodynamics

A.I. Ivanytskyi[a], K.A. Bugaev[a], E. G. Nikonov[b], E.-M. Ilgenfritz[c], D.R. Oliinychenko[a,d], V.V. Sagun[a,e], I.N. Mishustin[d,f], V.K. Petrov[a], G.M. Zinovjev[a]

[a]*Bogolyubov Institute for Theoretical Physics, National Academy of Sciences of Ukraine,Metrologichna str. 14[b], Kiev-03680, Ukraine*
[b]*Laboratory for Information Technologies, JINR, 141980 Dubna, Russia*
[c]*Bogoliubov Laboratory of Theoretical Physics, JINR, 141980 Dubna, Russia*
[d]*Frankfurt Institute for Advanced Studies (FIAS), Goethe-University, Ruth-Moufang Str. 1, 60438 Frankfurt upon Main, Germany*
[e]*CENTRA, Instituto Superior Técnico, Universidade de Lisboa, Av. Rovisco Pais 1, 1049-001 Lisboa, Portugal*
[f]*Kurchatov Institute, Russian Research Center, Akademika Kurchatova Sqr., Moscow, 123182, Russia*

arXiv:1606.04710v2 [hep-lat] 14 Feb 2017

Abstract

We apply the liquid droplet model to describe the clustering phenomenon in SU(2) gluodynamics, especially, in the vicinity of the deconfinement phase transition. In particular, we analyze the size distributions of clusters formed by the Polyakov loops of the same sign. Within such an approach this phase transition can be considered as the transition between two types of liquids where one of the liquids (the largest droplet of a certain Polyakov loop sign) experiences a condensation, while the other one (the next to largest droplet of opposite Polyakov loop sign) evaporates. The clusters of smaller sizes form two accompanying gases, and their size distributions are described by the liquid droplet parameterization. By fitting the lattice data we have extracted the value of Fisher exponent $\tau = 1.806 \pm 0.008$. Also we found that the temperature dependences of the surface tension of both gaseous clusters are entirely different below and above the phase transition and, hence, they can serve as an order parameter. The critical exponents of the surface tension coefficient in the vicinity of the phase transition are found. Our analysis shows that the temperature dependence of the surface tension coefficient above the critical temperature has a T^2 behavior in one gas of clusters and T^4 in the other one.

Keywords:
Key words: Polyakov loops, clusters, liquid droplet formula, surface tension, new order parameters
PACS:25.75.Nq, 25.75.-q

1. Introduction

The lattice formulation of quantum chromodynamics (QCD) is the only first principle tool which allows us to study the phase transformations between the confined and deconfined state of strongly interacting matter. Despite great successes of lattice QCD, up to now there is no complete understanding of the deconfinement phase transitions (PT) or crossover phenomena. A rich collection of results was obtained using the guidance of the Svetitsky-Jaffe hypothesis [1, 2]. This hypothesis links the deconfinement PT of a SU(N) pure gauge theory in (d+1)–dimensions to the magnetic transition in the corresponding d–dimensional symmetric

spin system being invariant under global center group Z(N)-transformations, actually in two versions: with SU(N) valued spins or with Z(N) valued spins. The role of spins [3] in the original SU(N) gauge theory is played by the so called local Polyakov loops, which can be interpreted as static quark sources with respect to the considered gauge theory.

The study of the deconfinement PT as a percolation process of clusters was advocated and started in [4, 5]. Recently this direction of research was continued [6, 7]. Despite many interesting findings, the authors of [6, 7] mainly concentrated on the properties of the largest and second largest 3-dimensional clusters formed by same-sign Polyakov loops and, hence, they did not pay attention to the properties of the multi-cluster structures made by smaller clusters. However, since the Fisher droplet model [8, 9] has been formulated, it became clear that there is no principal difference between the critical properties of liquid droplets in systems experiencing a liquid-gas PT on one hand and the properties of large spin domains in symmetric spin systems with a magnetization PT on the other hand. Note that exactly this similarity is able to naturally explain the fact that the critical exponents of ordinary simple liquids are the same as the critical indices of symmetric spin systems [8, 10, 11].

Further exploration of the properties of physical clusters has led to the formulation of several successful cluster models showing a first order PT [12, 13, 14, 15]. The Statistical Multifragmentation Model of atomic nuclei [12] treats the nuclear fragments of all sizes as charged droplets with a temperature dependent surface tension. Its exactly solvable version [15] differs from the Fisher model [8] mainly by the way of accounting for a hard-core repulsion between the nuclear fragments. It was a great surprise to learn that these two apparently similar models belong to different universality classes [16]. Also the Fisher droplet model [8] has been extended further in order to better reproduce the properties of real liquids [13, 14].

Another interesting development was made in [17], where the "gas of bag model" was formulated. In contrast to the usual cluster models [8, 12, 13, 14, 15], it did not take into account the surface tension of quark-gluon bags. Two generalizations of the "gas of bag model" which incorporate the surface tension for large quark-gluon bags [18, 19] were proposed and solved exactly. An inclusion of a surface tension which vanishes at certain values T_c of temperature and μ_c^B of baryonic chemical potential has allowed one to formulate statistical models with a first order deconfinement PT and/or a cross-over, between which there exists either a tricritical [18] or a critical endpoint [19] located at (T_c, μ_c^B). Actually, these models have naturally suggested a physical reason responsible for the degeneration of a first or second order PT into a cross-over. In [18] it was demonstrated that in the cross-over region the surface tension becomes negative and this very fact prevents the formation of the infinite cluster which otherwise would represent the liquid phase in all cluster models with first order PT. Because of the important role played by the surface tension, these models [18, 19] were named as "quark-gluon bags with surface tension" (QGBST).

Despite the success of the QGBST models in describing the critical exponents of some universality classes of spin systems such as the O(2)-O(4) model [20, 21] and a novel universality class called "the non-Fisher universality class" [22], it is clear that these phenomenological models are dealing with an oversimplified picture of quark-gluon bags.

Traditionally, in lattice QCD the deconfining PT is considered as a break down of discrete symmetry of a certain color group. In our opinion, however, such a language is more suited to study the liquid-solid or solid-solid PTs. From the heavy ion collision experiments we know that at low energy density the hadron phase is a mixture of gases [23], while at high energy densities achieved at modern colliders the QGP is the most perfect liquid (see e.g. [24]). Therefore, it would be more appropriate to consider the deconfinement PT as the liquid-gas one. On the other hand, from the discussion above it is also clear that without the essential

input from lattice QCD a further progress in developing cluster models for the deconfinement PT is simply impossible.

Therefore, in this work we would like to study the deconfinement PT in SU(2) gluodynamics on a finite lattice on the basis of cluster models [8, 15, 18, 19, 20, 21, 22, 25, 26] which describe the liquid-gas PT. For this purpose we will identify the geometrical clusters (a Íla Gattringer) formed from the local Polyakov loops (continuously valued spins) and study such important properties of the system as the value of the Fisher topological exponent τ and the temperature dependences of the reduced surface tension σ_A and of the reduced chemical potential μ_A which is usually generated in finite systems by the interaction between clusters [25, 26]. Also we would like to clarify the question what is the internal structure of the largest cluster which we consider as the gluon bag.

We consider the SU(2) gluodynamics on a finite lattice as a theoretical laboratory to study a well-known second order PT in a finite system with strong interaction and as a testing ground to verify the validity of the existing statistical models of cluster type to describe a non-Abelian gauge model. We restrict ourselves for this explorative study to SU(2) gluodynamics because this is the simplest and very well known non-Abelian gauge model and, hence, we hope to study in details the question on how the Z(2) symmetry breaking is reflected in changes of the collective properties of geometrical clusters formed by Polyakov loops. As it is shown below such an approach allowed us to introduce new order parameters and relate them to the mean value of Polyakov loop. Hence, we consider this work as the first attempt to reformulate lattice QCD thermodynamics into the language of statistical cluster models.

The work is organized as follows. In Section II we give the necessary definitions and recall the basic assumptions of the liquid droplet model. Section III is devoted to the discussion of the 4- and 3-parametric fits of the size distributions in the two types of cluster gases formed by the Polyakov loops. Such a fit allows us to determine the reduced surface tension of the clusters. The properties of the physical surface tension of the two types of clusters are discussed in Section IV. In Section V we calculate several critical exponents and explicitly demonstrate how the reduced surface tension coefficient can be used as an order parameter. Our conclusions are collected in Section VI.

2. A liquid droplet model parameterization for SU(2) gluodynamics

We have performed simulations of SU(2) on the fixed lattice with 4-dimensional volume $N_\sigma^3 \times N_\tau$, where $N_\sigma = 24$ and $N_\tau = 8$. Similarly to [6, 7] we introduce a cut-off value for the Polyakov loops $L_{cut} > 0$, whose convenience will be discussed later. The Polyakov loops were evaluated at each spatial base point of the 4-dimensional lattice. The lattice data were generated for 13 values of inverse coupling constant $\beta = \frac{4}{g^2}$ inside the interval $\beta \in [2.3115; 3]$. Here g^2 is the lattice QCD coupling constant. Since the lattice spacing a changes with β, i.e. $a(\beta)$, all the physical temperatures defined by $T = \frac{1}{N_\tau a(\beta)}$, are related to the 13 values of β in the investigated interval. The density of β points was chosen differently in different regions. Basically, if there are small changes in the observed distributions, we used a low density of β points, whereas on the high-temperature side of the phase transformation we used a higher density of β points. We emphasize that in contrast to the fixed scale approach, where one or few β values are chosen and the temperatures are changed by changing N_τ, the physical 3-dimensional volume of considered lattice changes with the temperature like $V \propto (1/T)^3$.

The main objects of our analysis are the size distributions of clusters formed by the Polyakov loops. The local Polyakov loop is real-valued for SU(2) gauge theory ranging from $+1$ to -1. For the cluster recognition we identify monomers, dimers, trimers and so on,

which are built from the neighboring Polyakov loops of the same sign (positive or negative, above some threshold). In contrast to the definitions used in works [6, 7], we prefer to use a terminology which is closer to the one used in studies of spin clusters of various spin models [27, 28, 29]. Instead of concentrating on the cluster of largest size, as in Refs. [6, 7], we analyze the clusters of all sizes and signs and treat them as finite liquid droplets. Since in the case of SU(2) gluodynamics the Polyakov loops of opposite signs are potentially different in their properties, here we investigate the size distributions of the clusters of both signs in order to elucidate the phenomenon of spontaneous Z(2) symmetry breaking. To distinguish them from each other we denote them as anticlusters and clusters, as defined later.

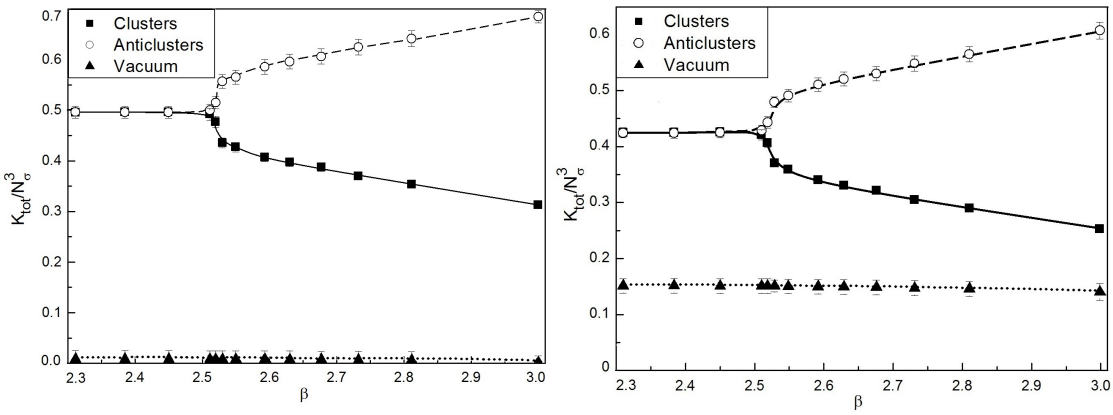

Figure 1: Total volume of clusters, anticlusters and auxiliary vacuum measured in units of 3-dimensional lattice cells a^3, relative to the full 3-dimensional volume, as functions of β. The auxiliary vacuum is independent of β. Results are shown for $L_{cut} = 0.1$ (left panel) and for $L_{cut} = 0.2$ (right panel). The curves are shown to guide the eye.

Let's first recall the formal definition of the local Polyakov loop. Traditionally, the volume average of the Polyakov loop is used as an order parameter in pure gauge theories. The local Polyakov loop $L(\vec{x})$, located at a spatial point with the coordinates $\vec{x}$, is defined by the trace of the product of temporal gauge links $U_4(\vec{x}, t)$

$$L(\vec{x}) = Tr \prod_{t=0}^{N_\tau - 1} U_4(\vec{x}, t)\,. \tag{1}$$

This expression shows that a local Polyakov loop is a gauge transporter which can be considered as the propagator of an infinitely heavy static quark at position $\vec{x}$ forward in time t. An important aspect is that the ensemble average of the spatially averaged Polyakov loop values is related to the free energy F_q of a single heavy quark as

$$\left\langle \frac{1}{V} \int d^3\vec{x} L(\vec{x}) \right\rangle \simeq \exp(-F_q/T)\,, \tag{2}$$

where T is the physical temperature of the system.

Similarly to Refs. [6, 7], the local Polyakov loop $L(\vec{x})$ located in a 3-dimensional point with coordinates $\vec{x}$ is counted as "spin up", if $L(\vec{x}) > L_{cut}$. Analogously, a Polyakov loop $L(\vec{x})$ is counted as "spin down", if $L(\vec{x}) < -L_{cut}$, whereas the Polyakov loops with intermediate values $-L_{cut} \leq L(\vec{x}) \leq L_{cut}$ are not accounted in the analysis and are regarded as an "auxiliary" ("confining") vacuum. Such a definition is convenient, since for a given cut-off the volume fraction of the auxiliary vacuum is independent of β value, as one can see from Fig. 1. A

given "spin up" is considered as a monomer, if all its nearest neighbors are either "spin down" or belong to the auxiliary vacuum. Similarly, two neighboring "spins up" form a dimer, if all their nearest neighbors are either "spin down" or belong to the auxiliary vacuum. In the same way one can define arbitrarily large n-mer for spins up and down. Besides a formal convenience, the cut-off L_{cut} plays an important role in studies of the thermodynamic limit on the lattice [7].

Let us call the largest n-mer on the lattice as the "anticluster droplet", whereas all other n-mers of the same spin sign (being smaller in size) are considered as the "gas of anticlusters". Similarly, let's call the largest n-mer of the opposite spin as a "cluster droplet", whereas other clusters of the same sign (which are smaller in size) are considered as a "gas of clusters". As one can see from Fig. 2, these definitions are sensible not only for each generated configuration of gauge fields, but also for the ensemble average over many configurations, because in most cases (except for highest values of β) the largest (anti)clusters are well separated from the corresponding gases. From Fig. 1 one can conclude that for a given cut-off the sum of cluster and anticluster volume fractions is β-independent and consequently the volume fraction of auxiliary vacuum is β-independent, too.

The average distributions n_k shown in Fig. 2 for the set of β-values have been calculated for ensembles of 800 and 1600 or 2400 independent configurations of gauge fields on the lattice. If the individual distributions found for 800 and 1600 independent configurations did not differ from each other within the statistical error bars, then we used the distribution averaged over 1600 configurations as high-statistics limit. In most cases such distributions have converged in the described sense, whereas for $\beta = 2.52$, $\beta = 2.53$ and $\beta = 2.677$ we were forced to enlarge the ensemble to 2400 independent configurations to calculate the averaged distributions. In fact, the configurations under analysis are separated by 10 Monte Carlo sweeps.

The size distributions of Fig. 2 are very similar to the ones found for 2- and 3-dimensional Ising systems [27, 28, 29] and to the nuclear fragment size distributions inside the mixed phase of a first order PT obtained within the statistical multifragmentation model [30] (see Figs. 5 and 6 therein). As one can see from Fig. 2, the typical structure of the size distributions of Polyakov loop clusters contains the following features:

1. A branch with average multiplicities monotonously decreasing with the cluster size which can be associated with the gas of clusters (and similarly for anticlusters) [12, 31, 32, 33, 34, 35, 29].
2. The largest cluster (anticluster) which is separated from the corresponding gas distribution by a gap and which, according to the liquid-gas PT phenomenology, can be associated with the corresponding liquid [12, 31, 32, 33, 34, 35, 29]. The distribution represents the fluctuations in size of largest (anti)cluster in different events.
3. The gap always exists for anticlusters, whereas for clusters it gradually becomes narrower for $\beta > 2.51$ while simultaneously the size distribution of the largest cluster evolves towards smaller sizes in such a way that at $\beta \simeq 3.0$ it gets inseparable from the size distribution characterizing the gas of clusters.

Based on the similarity of size distributions of Polyakov loop (anti)clusters and the ones of the Ising spin clusters and nuclear fragments, we decided to inquire whether the liquid droplet model (LDM) formula [8, 15]

$$n_A^{th}(k) = C_A \, \exp\left(\mu_A k - \sigma_A k^{\varkappa} - \tau_A \ln k\right) \, , \tag{3}$$

is able to reproduce the distributions of clusters (A=cl) and anticlusters (A=acl) found in the course of the Polyakov loop cluster analysis. As usual in cluster models [8, 13, 14, 15,

16, 20, 21, 22] the first term in the exponential on the right hand side of (3) defines the bulk free energy of k-volume (anti)cluster, the second term corresponds to a surface free energy of such (anti)cluster, while the last term represents the Fisher term with critical exponent τ_A. Fitting the (anti)cluster distributions, we can determine their reduced chemical potential μ_A (in units of temperature), the reduced surface tension coefficient σ_A (in units of temperature), the Fisher exponent τ_A and the normalization factor C_A. The true chemical potential and surface tensions are, respectively, defined as $T\mu_A$ and $T\sigma_A$.

Similarly to the 3-dimensional cluster models [8, 12, 13, 14, 15, 16, 20, 21, 22], the power $\varkappa$ relating the mean surface and mean volume of (anti)clusters was fixed by dimensionality to $\varkappa = \frac{2}{3}$. Fixing the value of the power $\varkappa$ in this way, we reduce the number of fitting parameters to 4 for each type of clusters. These parameters are C_A, μ_A, σ_A and τ_A with A=$\{$cl, acl$\}$. We are perfectly aware about the fractal dimension of large (anti)clusters [6, 36] and this is the reason why we do not fit the largest (anti)clusters in the system. On the other hand, the χ^2/dof values obtained by a four parametric fit are about 1 and this means that to leading order the effects of fractal dimension of the gas of (anti)clusters can be neglected.

3. Results of fit and their interpretation within the LDM-framework

Results of the 4-parametric fit. The first question to be clarified is to determine the minimal value of the (anti)cluster size k_{min}, for which the LDM parameterization (3) is valid. For instance, for 2-dimensional Ising clusters the minimal area was found to be 10 [29], while for 3-dimensional ones it was determined to be $k_{min} = 3$ [29].

The fit procedure corresponds to minimization of χ^2_A/dof

$$\frac{\chi^2_A}{dof} = \frac{1}{k_{max} - k_{min} - 4} \sum_{k=k_{min}}^{k_{max}} \frac{\left[n^{th}_A(k) - n_A(k)\right]^2}{\left[\delta n_A(k)\right]^2}, \tag{4}$$

with respect to parameters C_A, μ_A, σ_A and τ_A, independently for clusters (A=cl) and anticlusters (A=acl). Here the quantity $\delta n_A(k)$ denotes the statistical error in defining the average multiplicity $n_A(k)$ in simulations.

In practice, the minimization of χ^2_A/dof was done using the gradient search method. In other words, if the "vector of parameters" $\overline{p}_A = (C, \mu, \sigma, \tau)_A$ is known at some step of iteration procedure, then the next approximation is defined as

$$\overline{p}_A \to \overline{p}_A - \epsilon \cdot \nabla_{\overline{p}}\ \chi^2_A/dof. \tag{5}$$

Here $\nabla_{\overline{p}}$ is the gradient operator, whereas $\epsilon = diag(\epsilon_C, \epsilon_\mu, \epsilon_\sigma, \epsilon_\tau)$ is a diagonal matrix with positive elements. This simple scheme corresponds to the steepest descent search for the local extremum $\nabla_{\overline{p}}\chi^2_A/dof = 0$, where χ^2_A/dof has a minimum. It is necessary to stress that the obtained results demonstrate a high stability with respect to the random variation of the initial values of the parameters $\overline{p}_A$. For each minimization search 5 or 6 different initial values of the parameters $\overline{p}_A$ were taken randomly. If all of them led to the same minimum, the minimization was stopped. Hence, we are sure that the minima we have found are the global ones.

The upper limit k_{max} of the sum in Eq. (4) was chosen to account for the lattice data with a reliable statistics, i.e. when the statistical error of the k-volume (anti)cluster multiplicity $\delta n_A(k)$ is essentially smaller than the corresponding multiplicity $n_A(k)$. The maximal volume for which such a condition is satisfied is denoted as k_{max}. The (anti)clusters with the volume larger than k_{max} have been excluded from the fit procedure. The value of k_{max} depends

on β. For clusters defined with the cutoff $L_{cut} = 0.2$, the maximally admitted cluster size increases from $k_{max} \simeq 100$ for $\beta = 2.3115$ to $k_{max} \simeq 300$ for $\beta = 3.0$, whereas for anticlusters the maximally admitted cluster size gradually decreases from $k_{max} \simeq 100$ for $\beta = 2.3115$ to $k_{max} \simeq 10 - 20$ for $\beta = 3.0$. For clusters defined with the cutoff $L_{cut} = 0.1$ the corresponding range of k_{max} for clusters is between 50 at $\beta = 2.3115$ and 100 at $\beta = 3.0$, while for anticlusters it is between 50 at $\beta = 2.3115$ and $10 - 15$ (at most) at $\beta = 3.0$ (for more details see below).

Using the 4-parametric fit procedure for different values assumed for the minimal value of (anti)cluster volume $k_{min} \geq 1$, we found that only monomers ($k_{min} = 1$) are *not* described by the LDM formula (3). The mean deviation squared per number of degrees of freedom χ^2/dof are shown in Fig. 3 for several values of β. The results for other values of β are similar. Fig. 4 demonstrates the stability of the 4-parametric fit results obtained for $k_{min} = 2 - 4$ for clusters and for $k_{min} = 2 - 6$ for anticlusters.

The 4-parametric fit allowed us to simultaneously determine the k_{min} value for (anti)clusters and the range of values for the Fisher exponent τ. The traditional cluster models [8, 13, 14, 15, 16, 20, 21, 22] require a temperature independent value for the Fisher parameter τ. From Fig. 5 one can see that this requirement is well fulfilled both for clusters and anticlusters, if $k_{min} = 2$ is chosen. For $k_{min} = 3$ we see that values of τ found for different β differ significantly. Therefore, we conclude that the physically most adequate description of (anti)cluster sets of data can be achieved for $k_{min} = 2$. This conclusion is valid for both cut-off values studied here.

A few details should be given about finding the mean value of the Fisher index τ and its error. For $k_{min} = 2$ we obtain one β dependent set of the Fisher topological exponents for clusters and another set for anticlusters. Each of these two sets is characterized by the average value τ_A and its dispersion $\delta\tau_A$. It is remarkable that $k_{min} = 2$ simultaneously minimizes dispersions $\delta\tau_A$ for clusters and anticlusters. Our analysis shows that $\tau_{cl} \simeq 1.807$, $\delta\tau_{cl} \simeq 0.008$ and $\tau_{acl} \simeq 1.756$, $\delta\tau_{acl} \simeq 0.070$. According to the theory of measurements a common value of the Fisher topological exponent for clusters and anticlusters should be defined as the weighted average with the weights $\omega_A = 1/\delta\tau_A^2$, whereas its error is given by $\delta\tau = (\omega_{cl} + \omega_{acl})^{-1/2}$ [37]. Hence, we get $\tau_A \simeq 1.806 \pm 0.008$.

It is remarkable that in both these cases, i.e. for clusters and anticlusters, we have found $\tau_{cl} < 2$ and $\tau_{acl} < 2$ as the averaged values for different β. We believe this is an important finding because in Fisher droplet model one usually has $\tau > 2$ [8, 9], namely $\tau \simeq 2.07$ for the 2-dimensional case and $\tau \simeq 2.209$ for the 3-dimensional model. On the other hand, the value $\tau_A \simeq 1.806 \pm 0.008$ found here is consistent with the results of two exactly solvable cluster models considered in [16, 20, 22]. Note, that the question whether τ is larger or smaller than 2 is of principal importance because it determines the universality class of the model [16, 20, 21, 22].

Results of the 3-parametric fit. From the preceding discussion it is clear that now we can fix $k_{min} = 2$ and $\tau_A = 1.806 \pm 0.008$ and perform a fit of (anti)cluster distributions with only 3 parameters C_A, μ_A and σ_A with A=$\{$cl, acl$\}$. These results are presented in Fig. 6. One can see that the behavior of the LDM parameters C_A, μ_A and σ_A for clusters and anticlusters is identical up to $\beta \leq 2.5115$, while already for $\beta \geq 2.52$ the parameters of clusters and anticlusters behave differently. Such a difference is rooted in the symmetry breaking between the cluster and anticluster distributions which occurs due to the PT at the critical value of β, which in an infinite system is $\beta_c^{\infty} = 2.5115$ [38] for the lattice with $N_\tau = 8$.

Although the 3-parametric fit quality is overall good (see Fig. 6), for $\beta > 2.6$ we observe some fluctuations in the β-dependence of fitting parameters of anticlusters. Such a behavior is seen in Fig. 6 in the deviations of anticluster chemical potential, surface tension and

normalization constant from the regular curves. On the other hand, the behavior of the cluster fitting parameters is perfectly regular. The main reason for such a difference between clusters and anticlusters at $\beta > 2.6$ is that – compared to monomers and dimers – the multiplicities of anticlusters with $n > 3$ are extremely small and hence they experience strong statistical fluctuations from one lattice configuration to another. As a result for these values of β a reliable statistics exists for the gas of anticlusters, if their volume is up 10–15 elementary lattice cubes. This is clearly seen, if one compares the anticluster size distributions for $\beta = 2.53$ and $\beta = 3.0$ shown in Fig. 2 for the cut-off $L_{cut} = 0.2$. For the cut-off $L_{cut} = 0.1$ the statistics for the gas of anticlusters with size larger than 10 units is even less reliable at $\beta > 2.6$ due to their very small multiplicities. Due to this reason in the present work the main attention is paid to the analysis of the lattice results obtained for the cut-off $L_{cut} = 0.2$, while in appropriate places we comment in what respect the results obtained for the cut-off $L_{cut} = 0.1$ differ from the ones found for $L_{cut} = 0.2$.

Already from Figs. 2 and 6 one can see that the real situation in SU(2) gluodynamics is much more complicated than just a percolation of a largest anticluster. The physical picture can be well formulated in terms of two "substances" which are represented by gases of clusters and anticlusters and their respective liquids, i.e. the largest cluster and anticluster. The behavior of the reduced chemical potentials μ_A in Fig. 6 shows that at $\beta \leq \beta_c^{\infty}$ these two "substances" are in chemical equilibrium, while at $\beta > \beta_c^{\infty}$ it gets lost. This conclusion is further substantiated in Figs. 7 and 8 which show the mean size of (anti)clusters in the respective gas, $\langle k_A \rangle_{gas}$, the mean size of all (anti)clusters $\langle k_A \rangle_{tot}$ and the mean size of the largest (anti)clusters. The latter is calculated numerically as

$$\max K_A = \frac{\sum\limits_{k=1} k^{1+\tau_A} \, n_A^{lat}(k)}{\sum\limits_{k=1} k^{\tau_A} \, n_A^{lat}(k)} \, , \tag{6}$$

where $n_A^{lat}(k)$ is the multiplicity of lattice clusters of A-type and volume k, while the value of τ_A coincides with the one found from the 4-parametric fit $\tau_A = 1.806 \pm 0.008$. Numerically we have verified that Eq. (6) correctly defines the mean size of the largest (anti)cluster for the whole range of β values under investigation.

From Fig. 7 one can immediately see that above β_c^{∞} the anticluster liquid droplet accumulates the gas particles while the cluster liquid droplet evaporates them. Below β_c^{∞} the main contribution to both gases is given by monomers, dimers and trimers. Above β_c^{∞} the gas of clusters gains sizable contributions from 4-, 5- and 6-mers, while the gas of anticlusters quickly degenerates into a mixture of monomers and dimers, at most. It is clear that the bifurcation singularity at $\beta = \beta_c^{\infty}$ which is visibly seen in Figs. 6-8 can be identified as the critical point for the 2-nd order PT (see further discussion in Sect. V).

Note that exactly solvable models dealing with a 1-st order PT [15, 17], when rigorously analyzed in a finite volume [25, 26], predict that (i) in a finite system the analog of a PT must occur at positive values of the effective chemical potential and that (ii) the analog of mixed phase in a finite system consists of states which are *not* in chemical equilibrium with each other. Both of these statements are valid also in case of a tricritical endpoint, at which a 1-st order PT degenerates into a 2-nd order one. Therefore, the predictions of Refs. [25, 26] look very similar to what we find here for the behavior of the reduced chemical potentials μ_A of (anti)clusters (see Fig. 6). However, there is a principal difference between the solutions found in [25, 26], where the chemical equilibrium is lost between the gas of all clusters (stable state) and metastable states of the same "substance" [25, 26], and the present model, where

the chemical equilibrium is apparently lost between the two "substances", i.e. two gases, as follows from the different behavior of their reduced chemical potentials μ_A shown in Fig. 6.

4. Discussion of physical surface tension

The second principal difference between the present and the other cluster models [8, 12, 13, 14, 15, 16, 18, 19, 20, 21, 22, 30] is an entirely different temperature behavior of the surface tension. In traditional cluster models the surface tension is a decreasing function of the temperature, and it vanishes at the (tri)critical endpoint temperature T_{end}. At temperatures above T_{end} the surface tension of existing models is either zero as in [8, 12, 13, 14, 15, 16] or it becomes negative as in [18, 19, 20, 21, 22, 30]. As one can see from Fig. 6 and more clearly from Fig. 9 the surface tension of (anti)clusters does not vanish at β_c^∞ and above it. In the present analysis (with fixed N_τ), the physical temperature is a monotonically increasing function of β (see Table I for details) [39] and, hence, our comparison of β-dependencies shown in these figures is justified. [1]

Table 1: Two-loop β dependence of the spatial lattice spacing $a_\sigma(\beta)$ given by the ratio to $a_\sigma(\beta_c^\infty)$ as function of the physical temperature T in units of the critical temperature T_c^∞.

β	$a_\sigma(\beta)/a_\sigma(\beta_c^\infty)$	T/T_c^∞
2.3115	1.7132	0.5837
2.3850	1.4057	0.7114
2.4500	1.1783	0.8487
2.5115	1.0000	1.0000
2.5200	0.9774	1.0231
2.5300	0.9514	1.0510
2.5500	0.9016	1.1092
2.5930	0.8030	1.2453
2.6300	0.7269	1.3757
2.6770	0.6405	1.5612
2.7325	0.5516	1.8128
2.8115	0.4459	2.2423
3.0000	0.2685	3.7244

The β-dependence of physical surface tension defined as

$$\sigma_A^{phys}(\beta) \;\equiv\; T\frac{\sigma_A(\beta)}{[\,a_\sigma(\beta)\,]^2} \;= T_c^\infty\;\frac{a_\sigma(\beta_c^\infty)}{a_\sigma(\beta)}\frac{\sigma_A(\beta)}{[\,a_\sigma(\beta)\,]^2}\,, \tag{7}$$

where in the last step we have used the following relation for the temperature $T = T_c^\infty \frac{a_\sigma(\beta_c^\infty)}{a_\sigma(\beta)}$ [39]. Such a surface tension has the correct physical dimension, but it is more convenient to use the dimensionless ratio $\sigma_A(\beta)\,a_\sigma(\beta_c^\infty)/\sigma_A(\beta_c^\infty)/a_\sigma(\beta)$ because such a ratio, as one can see from Fig. 9, clearly demonstrates the different behavior on two sides of the point $\beta = \beta_c^\infty$. Also in this case one does not need to care about an exact value of a coefficient relating the

[1] The values of physical temperature shown in Table I are calculated in a standard way using the two loop formula [39]. Although below β_c^∞ such an approximation can be used for a restricted range of values of the inverse coupling constant squared β, it is a good approximation above β_c^∞.

volume and the surface of (anti)clusters. To find this ratio from Eq. (7) we used the second column of Table I.

We would like to stress that in contrast to all known cluster models the physical surface tension of clusters has a peak at about β_c^∞ while the surface tension of anticlusters has a kink at this point. Also both of them show a jump of the derivative with respect to β and, hence, a jump of the derivative with respect to T, on two sides of the point $\beta = \beta_c^\infty$. Such a behavior of the surface tension would be rather unusual for the 1-st order liquid-gas PT in traditional cluster models [8, 12, 13, 14, 15, 16, 20], whereas it was recently suggested in [19] as a mechanism of a surface-tension induced deconfining transition in a phenomenological model constructed with the aim to explain a PT in QCD with a critical endpoint. However, in contrast to the present findings, the deconfined phase in the model of [19] has a negative surface tension. Also it is necessary to remember that for most of existing cluster models with a 1-st order PT of liquid-gas type there is no jump of T-derivative of surface tension on two sides of the (tri)critical endpoint temperature T_{end}, where the 1-st order PT changes into a 2-nd order PT. There are two well established exceptions presented by models which have a critical endpoint, namely the Fisher droplet model [8] and the QGBST model [19, 20, 21]. But both these models are valid for the Fisher exponent value $\tau > 2$, while the present model, derived from SU(2) gluodynamics, has a clearly different Fisher exponent $\tau_A \simeq 1.806 < 2$.

The fact that in the vicinity of critical temperature $T = T_c^\infty$ the physical surface tension of (anti)clusters does not vanish is in contrast with the traditional belief of the cluster models that at the critical or tricritical endpoint there should exist the power law in the size distribution of physical clusters. In the present study we see that the anticlusters do not show any power law at any β, while the power law of the size distribution of clusters is seen at $\beta = 3.0$, i.e. at very high temperature.

This leads us to the first important conclusion of the present work. Our analysis of the SU(2) Polyakov loop clusters and anticlusters demonstrates that none of existing cluster models of the liquid-gas PT can be used to safely interpret the results. Our discussion above shows that the gases of clusters and anticlusters have a few common features with some of the models, but their main properties such as the surface tensions and the apparent absence of chemical equilibrium above T_c^∞ cannot be described by existing models. Therefore, the new properties of the gases of clusters and anticlusters in SU(2) gluodynamics require a development of a new cluster model which differ from the existing ones.

From Fig. 9 one can also see that the behavior of the normalized surface tension of (anti)clusters is rather similar for both values of the cut-off parameter. Of course, there is no absolutely identical behavior, but, first of all, this is caused by essentially smaller statistics of data studied with $L_{cut} = 0.1$ (especially for anticlusters). Secondly, all quantities referring to clusters and anticlusters, if normalized to their values at β_c^∞, demonstrate a very similar behavior as function of β for both cut-offs. Apparently, the list of such quantities includes not only μ_A, σ_A and C_A, but also the average volume of (anti)clusters in the gas phase, $\langle k_A \rangle_{gas}$ (see Fig. 7), as well as their total average volume $\langle k_A \rangle_{tot}$ (see Fig. 7) including the largest clusters of both kinds, as well as the mean volume of the largest clusters of both kinds defined by Eq. (6). To illustrate the convenience of normalized quantities once more, in Fig. 10 we show the behavior of properly scaled normalization factor C_A

$$\frac{C_A^{phys}(\beta)}{C_A^{phys}(\beta_c^\infty)} \equiv \frac{C_A(\beta)}{C_A(\beta_c^\infty)} \left[\frac{a_\sigma(\beta_c^\infty)}{a_\sigma(\beta)}\right]^3 . \tag{8}$$

Such a choice is made in order to get the particle number density of k-volume (anti)clusters $\rho_A(k)$. To find it one has to divide the multiplicity of k-volume (anti)clusters, $n_A^{lat}(k)$, observed

on the lattice by the system volume $V = [N_\sigma\, a_\sigma(\beta)]^3$. In this case the normalization factor $C_A(\beta)$ in physical units acquires the form (8). Fig. 10 demonstrates that in physical units the normalization factors of clusters which are found for two cut-off values are practically identical, while for anticlusters they slightly differ at high values of β at which the statistics for a cut-off $L_{cut} = 0.1$ gets rather poor. Also this figure shows that in physical units the kink in the β dependence of normalization factor C_A^{phys} is hardly noticeable.

Note, that according to the definition (4) the normalization factor C_A^{phys} in physical units C_A^{phys} has a meaning of thermal density of k-volume (anti)clusters per one internal degree of freedom (i.e. the total particle number density per one internal degree of freedom at $\mu_A = 0$), while the factors depending on σ_A and τ in (4) determine the number of internal degrees of freedom [8]. As one can see from Fig. 6, the normalization factor of anticlusters C_{acl} already saturates at $\beta = 2.7$, while such a quantity for clusters C_{cl} shows a weak linear growth for $\beta \geq 2.7$. However, by changing β from 2.81 to 3.0 we increase C_{cl} by 10%, while the physical temperature is increased by 66%. Thus, there is a very weak linear temperature dependence of C_{cl} at $T/T_c^\infty \geq 2.24$, which can be safely ignored. One can make a rough estimate of the temperature dependence power for the clusters noting that the ratio $\frac{C_{cl}^{phys}(\beta)}{C_{cl}^{phys}(\beta_c^\infty)}$ changes in 500 times (see left panel of Fig. 10), while temperature increases in about 6.3 times. Then the desired power for clusters is $\frac{\ln(500)}{\ln(6.3)} \simeq 3.3$. For the anticlusters one can estimate this power by considering a change of the ratio $\frac{C_{acl}^{phys}(\beta)}{C_{acl}^{phys}(\beta_c^\infty)}$ within the interval $\beta \in [2.3115, 2.8115]$ at which the temperatures increases in about 3.84 times. From the right panel of Fig. 10 one finds that this power for anticlusters is $\frac{\ln(50)}{\ln(3.84)} \simeq 2.9$.

From these estimates we conclude that at high temperatures, i.e. for $1.25\, T_c^\infty < T \leq 3.7\, T_c^\infty$, the normalization factor C_A^{phys} in physical units behaves similarly to the particle number density in ultrarelativistic gas (a gas of massless particles), i.e. as $C_A^{phys} \sim T^3$. Note that the only massless particles which exist in gluodynamics are the gluons, whose thermal density behaves as T^3 [40], although the gluons were not explicitly considered in our study. Thus, we believe it is remarkable that information about massless gluons is implicitly encoded in the density of Polyakov loop (anti)clusters.

Now we would like to discuss some physical consequences of the temperature dependence of the surface tension of clusters and anticlusters. Although in the present work we do not investigate the thermodynamic limit of the LDM parameterization, we can draw certain conclusions on the temperature dependence of cluster properties. The importance of the surface tension of quark-gluon (QG) bags was realized a long time ago [41, 42, 43]. However, despite of many efforts to calculate this quantity in the modern literature, the predicted surface tension of QG bags at zero temperature ranges from 5-15 MeV/fm^2 [44, 45] to about 150 MeV/fm^2 [46, 47] or even 300 MeV/fm^2 [48]. Also it is not much known about the QG bag surface tension behavior at high temperatures [46, 47]. Without studying the thermodynamic limit of the present approach, we cannot fix an absolute magnitude of the coefficient in Eq. (7) for the physical surface tension. However, the present approach allows us to predict the functional T-dependence of the physical surface tension of Polyakov loop clusters

$$\sigma_{cl}^{phys}(T) \;=\; \frac{Const}{[\,a_\sigma(\beta)\,]^2} \;\sim\; T^2 \quad \text{for} \quad 1.25\, T_c^\infty < T \leq 3.7\, T_c^\infty\,. \tag{9}$$

The validity of this estimate is clearly seen from Fig. 9, which demonstrates that the ratio $\sigma_{cl}(\beta)\, a_\sigma(\beta_c^\infty)/\sigma_{cl}(\beta_c^\infty)/a_\sigma(\beta)$ saturates at $\beta \geq 2.6$. Also we found the following estimate $\sigma_{acl}^{phys}(T) \;\sim\; T^4$ for the physical surface tension of anticlusters at temperatures belonging to the range $1.25\, T_c^\infty < T \leq 3.7\, T_c^\infty$. However, one should keep in mind that, in contrast to

clusters, for which $\mu_{cl} \to 0$ in this temperature range, the quantity $\sigma_{acl}^{phys}(T)$ may also include an unknown dependence on reduced chemical potential μ_{acl}, which for anticlusters strongly increases with T (see Fig. 6).

One important difference between the present consideration and the traditional cluster models is that the largest Polyakov loop cluster (anticluster) is not homogeneous inside and it looks like a Swiss Cheese, since it is filled by the gas of anticlusters (clusters). A similar conclusion for the largest anticluster was recently suggested in [49]. Note, however, that in traditional cluster models, including the Fisher droplet model [8], such a possibility is usually ignored. Let us demonstrate this important new feature for the cut-off $L_{cut} = 0.2$ and $\beta = 3.0$. At high values of β the treatment gets simpler, since the gas of anticlusters is practically absent and the largest cluster is rather small. Indeed, for $\beta = 3.0$ one finds that the volume of largest anticluster is $\max K_{acl} = 7300$, the volume of largest cluster is $\max K_{cl} = 223$, the total volume of the gas of anticlusters is only $V_{acl}^{gas} = \widetilde{\sum_k} k\, n_{acl}(k) = 89$, while the total volume of the gas of clusters is $V_{cl}^{gas} = \widetilde{\sum_k} k\, n_{cl}(k) = 2848$ and the volume of auxiliary vacuum is $V_{vac} = 1707$. Hereafter the sums with tilde indicate that the summation does not include the largest (anti)cluster. In order to find out where the gaseous clusters are located, let us first estimate the number of nearest neighbors for the gas of clusters. Since in the gas of clusters the number of monomers is $n_{cl}(1) \simeq 550$, the number of dimers is $n_{cl}(2) \simeq 130$ and the number of trimers and fourmers are, respectively, $n_{cl}(3) \simeq 60$ and $n_{cl}(4) \simeq 35$, then one can estimate the number of their nearest neighbors as $N_{cl}^{near} \simeq 6\, n_{cl}(1) + 10\, (n_{cl}(2) + n_{cl}(3) + n_{cl}(4)) \simeq 5600$. Here we have taken into account that each monomer has 6 nearest neighbors, each dimer has 10 nearest neighbors, while the larger clusters have at least 10 nearest neighbors. According to definition, the nearest neighbors of a gaseous cluster cannot be the other gaseous clusters themselves or the largest cluster, but should be only the anticlusters or vacuum. However, the gas of anticlusters is practically absent at $\beta = 3.0$, while the vacuum can provide maximum 1707 nearest neighbors out of about 5600. Therefore, the gas of clusters must be located inside the largest anticluster, since it is the only possibility to locate them.

Evidently, the number of nearest neighbors given above is somewhat overestimated. One can find it differently. Suppose that there is a dense packing of gaseous clusters among the vacuum and anticlusters. The dense packing for monomers, evidently, means that they are surrounded by the monomers of vacuum or/and anticlusters, i.e. the volume of surrounded matter N_1^{surr} in this case equals to the number of cluster monomer $N_1^{surr} = n_{cl}(1) \simeq 550$. The volume of matter which surrounds all larger clusters can be found from the expression

$$N_2^{surr} \simeq \sum_{2}^{\max K_{cl}} \frac{S(k)}{2}\, n_{cl}(k) \simeq 2550\,, \tag{10}$$

where $\max K_{cl} = 223$ is the size of largest cluster at $\beta = 3.0$, $n_{cl}(k)$ is the number of clusters of volume k, $S(k) = c_s\, k^{\frac{2}{3}}$ is the surface of a cluster of volume k, while the coefficient $c_s \simeq 4.83$ relates the surface of sphere to its volume. Note that such a treatment is justified by the validity of the LDM formula. It is also evident that considering all clusters with the volume $k \geq 2$ as spheres we can estimate N_2^{surr} from below, since for a given volume a spherical form provides a minimal surface. In (10) the coefficient $\frac{1}{2}$ accounts for the fact that for dense packing only a half of a surrounding volume "belongs" to a given cluster, while the other half "belongs" to the other cluster. In other words, this coefficient allows one to avoid the double counting of the same surrounding volume separating two neighboring clusters.

Summing up N_1^{surr} and N_2^{surr} one can find the total surrounding volume for all clusters $N_{tot}^{surr} \simeq 3100$. Even in this extreme case the vacuum and small gaseous anticlusters can

together surround only 1707+89 = 1796 units of volume of gaseous clusters, while the remaining number of gas clusters should be located inside the largest anticluster, i.e. the latter should resemble the Swiss Cheese. Hence, we come to the same conclusion again. Note that in this case the relative packing fraction of gaseous clusters inside the largest anticluster is $\rho_{cl/acl} = V_{cl}^{gas} / \max K_{acl} \simeq 0.39$, i.e. our previous assumption about the dense packing was too strong.

It is evident that the gas of clusters did not exclusively appear inside the largest anticluster at $\beta = 3.0$, but this gas existed inside of it at all temperatures. Similarly, the gas of anticlusters exists inside the largest cluster at all values of β. These conclusions naturally explain that by increasing β above β_c the volume of gas of clusters increases simultaneously with the growth of $\max K_{acl}$ and that in this case the volume of gas of anticlusters decreases simultaneously with the reduction of $\max K_{cl}$. For $\beta = 3.0$ this statement can be nicely illustrated using the following estimates. Indeed, comparing the relative packing fraction of the gaseous anticlusters inside the largest cluster $\rho_{acl/cl} = V_{acl}^{gas} / \max K_{cl} \simeq 0.399$ and the one of the gaseous clusters inside the largest anticluster $\rho_{cl/acl} \simeq 0.39$, one finds almost the same values. In addition, an existence of the Swiss Cheese structure would naturally explain the fact of the fractal dimension of the largest (anti)clusters [6, 36]. Therefore, one should distinguish between the volume of the largest (anti)cluster and its geometrical size, which can be essentially larger, than its volume due to presence of the non-native gas. Hence, the surface free energy of the largest (anti)cluster should have the following form

$$F_A^{surf} = \Sigma_A^{outer} \left[\max K_A + \widetilde{\sum_k} k \, n_{\bar{A}}(k) \right]^{\frac{D_A - 1}{D_A}} - T \sigma_{\bar{A}} \widetilde{\sum_k} k^{\frac{2}{3}} \, n_{\bar{A}}(k) \, , \tag{11}$$

where the notation $\bar{A}$ means the summation over the gaseous clusters which are non-native for the largest cluster of sort A and D_A is its fractal dimension [49]. The first term on the right hand side accounts for the outer surface of maximal (anti)cluster containing the non-native gas with the outer surface tension coefficient Σ_A^{outer}, while the second term on the right hand side of (11) accounts for the surface free energy of all cavities made by the non-native clusters. Now it is also clear that non-native gas may exist inside the (anti)clusters which are smaller than the largest one.

Another important observation related to the surface free energy of the largest anticluster is that at large values of β it becomes negative. This is easy to understand, if one recalls that at such values of β the largest anticluster practically occupies the whole lattice. Since in all spatial directions the lattice fields have the periodic boundary conditions, the surface of largest anticluster has no outer borders (since it has the borders with itself only). Due to this reason the first term on the right hand side of Eq. (11) is absent at large values of β (or at high temperatures in our formulation) and, therefore, its surface free energy becomes negative, i.e. $F_{acl}^{surf} < 0$. Note that appearance of negative surface free energy of largest anticluster might be important for understanding the reason of cross-over appearance in full QCD at low baryonic densities [18, 19, 50, 51].

5. Surface tension coefficient as a new order parameter

From Figs. 6-9 one can immediately learn that in the phase of unbroken $Z(2)$ symmetry, i.e. for $\beta \leq \beta_c^{\infty}$, the behavior of the thermodynamical functions μ_A, σ_A, C_A, $\langle k_A \rangle_{gas}$, $\langle k_A \rangle_{tot}$ and $\max K_A$ for clusters and anticlusters is absolutely identical within the error bars, while

in the phase of broken $Z(2)$ symmetry these functions are entirely different. Therefore, one can use the following combination

$$P_q = \left| \frac{q_{acl} - q_{cl}}{q_{acl} + q_{cl}} \right| , \tag{12}$$

for any of the quantities $q_A \in \{\mu_A, \sigma_A, C_A, \langle k_A \rangle_{gas}, \langle k_A \rangle_{tot}, \max K_A\}$ as an order parameter of PT between the phases with unbroken and broken symmetry. We, however, would like to show that from the present results obtained for finite systems one can extract a more detailed physical information.

In order to show this, first we have to discuss the traditional order parameter, i.e. the spatial average of the local Polyakov loop $\langle L(\vec{x}) \rangle$. Evidently, one can identically rewrite the average over all spatial points as an average over all clusters and anticlusters

$$\langle L(\vec{x}) \rangle \equiv \frac{\sum\limits_x L_x}{N_\sigma^3} = \frac{\sum\limits_{acl} |L_k^{acl}|\, k\, n_{acl}(k) - \sum\limits_{cl} |L_k^{cl}|\, k\, n_{cl}(k)}{N_\sigma^3} = \\ \frac{\widetilde{\sum\limits_k} \left[|L_k^{acl}|\, k\, n_{acl}(k) - |L_k^{cl}|\, k\, n_{cl}(k) \right] + |L_{max}^{acl}| \max K_{acl} - |L_{max}^{cl}| \max K_{cl}}{N_\sigma^3} , \tag{13}$$

where $|L_k^{cl}|$ and $|L_k^{acl}|$ denote, respectively, the modulus of mean value of Polyakov loop inside clusters and anticlusters of volume k. In the last equality we used the sum over the volumes of all (anti)clusters except for the largest one, which are added explicitly. In doing so we accounted for the fact, that the largest (anti)cluster is always a single one. For definiteness, in Eq. (13) we defined $\langle L(\vec{x}) \rangle$ in such a way that in thermodynamic limit it vanishes at and below β_c^∞, but is positive above β_c^∞. Eq. (13) shows that vanishing of $\langle L(\vec{x}) \rangle$ in the symmetric phase is provided by the set of inequalities

$$|L_k^{acl}| + |L_k^{cl}| \;\gg\; \left| |L_k^{acl}| - |L_k^{cl}| \right| , \tag{14}$$

$$n_{acl}(k) + n_{cl}(k) \;\gg\; |n_{cl}(k) - n_{acl}(k)| , \tag{15}$$

which are valid for all volumes $k \geq 1$. Note that in finite systems, which we study here using the lattice data with limited statistics, the right hand sides of Eqs. (14) and (15) do not always vanish for $k \gg 10$, but the multiplicity of such (anti)clusters is so small compared to monomers or dimers (about 4-6 order of magnitude as one can see from Fig. 2) that one can safely ignore them in the sums marked with tilde in Eq. (13).

In the upper vicinity of β_c^∞ the inequality (14) remains valid, while the inequality (15) breaks down already for monomers and dimers, as one can deduce from Fig. 11. This figure indicates that changing β from $\beta_c^\infty = 2.5115$ to 2.52, i.e. by about 0.4%, one obtains a sizable change of the asymmetry of cluster-anticluster multiplicity even for small (anti)cluster volumes $k \leq 10$. Such an asymmetry can be expressed in the form of Eq. (12) for $q_A = n_A(k)$, Therefore, Eq. (13) can be further approximated in the vicinity of β_c^∞ as

$$\langle L(\vec{x}) \rangle \;\simeq\; \frac{\widetilde{\sum\limits_k} \left[|L_k^{acl}| + |L_k^{cl}| \right] k\, (n_{acl}(k) - n_{cl}(k)) + \left[|L_{max}^{acl}| + |L_{max}^{cl}| \right] (K_{max}^{acl} - K_{max}^{cl})}{2\, N_\sigma^3} \tag{16}$$

$$\simeq\; \frac{\left[|L_{max}^{acl}| + |L_{max}^{cl}| \right] (K_{max}^{acl} - K_{max}^{cl})}{2\, N_\sigma^3} , \tag{17}$$

where in the last step both sums over all (anti)cluster volumes were neglected compared to two contributions of the largest ones. This is a good approximation, since in the vicinity of

β_c^∞ the total volume occupied by the gases of clusters and anticlusters is only a few percents of the corresponding liquid droplet. Therefore, in calculating the mean value of Polyakov loop (13) we could from the very beginning perform a summation only over the largest cluster and anticluster. Eq. (17) shows that in the vicinity of β_c^∞ the volume average of the Polyakov loop $\langle L(\vec{x})\rangle$ of SU(2) gluodynamics is dominated by the difference between the mean volume of largest anticluster and the mean volume of largest cluster.

Based on the analogy between the volume average of the Polyakov loop in SU(2) gluodynamics and the spontaneous magnetization in the $Z(2)$ 3-dimensional spin model, we have studied the behavior of two additional order parameters in the upper vicinity of β_c^∞. The first of them is the difference

$$\Delta \max K_A(\beta) = \max K_A(\beta) - \max K_A(\beta = 2.52)\,. \tag{18}$$

From Fig. 8 one immediately can deduce that for the largest anticluster $\Delta \max K_{acl}(\beta) \geq 0$ for $\beta \geq 2.52$, while for the largest cluster $\Delta \max K_{cl}(\beta) \leq 0$ for $\beta \geq 2.52$. In order to determine the behavior of the difference (18) in the vicinity of transition region, we fitted it with two parameters a_A and b_A using the formula

$$\Delta \max K_A(\beta \geq 2.52) = \pm a_A \cdot (\beta - 2.52)^{b_A}\,, \tag{19}$$

where the sign + (−) corresponds to $A = acl$ ($A = cl$). Note that such an expansion for the right hand side vicinity of $\beta = 2.52$ was chosen because this point, indeed, belongs to the transition region, as one can see from Figs. 8 and 11, while in our finite system the states which correspond to the point $\beta = \beta_c^\infty$ still belong to the phase with unbroken symmetry. The results of fit are presented in Table II.

Table 2: The fit parameters according to Eq. (19).

cut-off	type	a_A	b_A	χ^2/dof
$L_{cut} = 0.1$	clusters	3056 ± 246	0.2964 ± 0.0284	$16.32/4 \simeq 4.08$
$L_{cut} = 0.1$	anticlusters	2129 ± 160	0.3315 ± 0.0269	$8.94/4 \simeq 2.235$
$L_{cut} = 0.2$	clusters	4953 ± 443	0.3359 ± 0.0289	$12.3/3 \simeq 4.01$
$L_{cut} = 0.2$	anticlusters	2462 ± 87.7	0.3750 ± 0.0129	$2.068/4 \simeq 0.517$

During the fitting we employed the data for 4, 5, 6, 7, 8 and 9 values of β for each quantity analyzed. Then we have chosen those sets, which provide the minimal value of χ^2/dof. Usually, these were 6 values of β beginning at $\beta = 2.52$, but in one case the lowest value of χ^2/dof was achieved for five points (see the fourth row from above in Table II). Although in some cases the obtained χ^2/dof values are somewhat large, the overall quality of the data description is good, as one can see from the curves depicted in Fig. 8. The obtained large χ^2/dof values can be easily understood, if one takes into account rather small statistical errors and the finite, and not large, size of the system under investigation. It is, nevertheless, remarkable that the found exponents b_A from Table II are very close to the critical exponent $\beta_{\rm Ising} = 0.3265 \pm 0.0001$ [52] of 3-dimensional Ising model and to the critical exponents $\beta_{\rm liquids} = 0.335 \pm 0.015$ [53] of simple liquids, although the exponent b_{acl} for the cut-off $L_{cut} = 0.2$ is somewhat larger.

Now we investigate the β-behavior of the reduced surface tension coefficients $\sigma_A(\beta)$ using the following difference

$$\Delta\,\sigma_A(\beta \geq 2.52) = \sigma_A(\beta) - \sigma_A(\beta = 2.52) = \pm d_A \cdot (\beta - 2.52)^{B_A}\,, \tag{20}$$

which we expanded in the right hand side vicinity of the point $\beta = 2.52$ similarly to Eq. (19). In Eq. (20) the sign + (−) again corresponds to $A = acl$ ($A = cl$). The constants d_A and B_A were found similarly to the case of the fitting the largest cluster β-dependence with Eq. (19). With one exception the lowest values of χ^2/dof were achieved for six values of $\beta \in [2.52; 2.677]$. However, we found that anticlusters for the cut-off $L_{cut} = 0.2$ reach minimal value χ^2/dof for four values of β (see the lowest raw in Table III). The obtained results are given in Table III, which also shows that the quality of the fit is better than for Eq. (19). The curves representing Eq. (20) with the best parameters are shown in Fig. 6. We can notice that the parameterization (20) perfectly describes the reduced surface tension of clusters for all values of $\beta \geq 2.677$, i.e. outside the range of fitting. This one can see in Fig. 6 for the cut-off $L_{cut} = 0.2$. The situation for the cut-off $L_{cut} = 0.1$ is absolutely the same.

From Table III one can see that the values of exponents B_{acl} for gas of anticlusters are (within error bars) close to 0.5, while the exponents B_{cl} for the gas of clusters are close to 0.29. In other words, within error bars the exponents B_{cl} are close to the critical exponent $\beta_{\rm Ising}$ of 3-dimensional Ising model, while B_{acl} are close to the critical exponent of mean-field models $\beta_{\rm mf} = 0.5$. The large difference between values of B_{acl} and B_{cl}, however, requires an explanation. Our educated guess is that the exponents B_{acl} for anticlusters are affected by the large values of their chemical potential.

Table 3: The fit parameters according to Eq. (20).

cut-off	type	d_A	B_A	χ^2/dof
$L_{cut} = 0.1$	clusters	0.485 ± 0.014	0.2920 ± 0.0012	$1.43/4 \simeq 0.36$
$L_{cut} = 0.1$	anticlusters	2.059 ± 0.028	0.4129 ± 0.0077	$1.68/4 \simeq 0.48$
$L_{cut} = 0.2$	clusters	0.2796 ± 0.0118	0.2891 ± 0.0016	$1.11/4 \simeq 0.28$
$L_{cut} = 0.2$	anticlusters	1.344 ± 0.033	0.4483 ± 0.0021	$0.66/2 \simeq 0.33$

From Eqs. (19) and (20) one can obtain two scaling laws relating $\max K_A(\beta)$ and $\sigma_A(\beta)$ in the right hand side vicinity of the point $\beta = 2.52$

$$\left|\frac{\max K_A(\beta) - \max K_A(2.52)}{a_A}\right|^{\frac{1}{b_A}} = \left|\frac{\sigma_A(\beta) - \sigma_A(2.52)}{d_A}\right|^{\frac{1}{B_A}} . \qquad (21)$$

These scaling laws allow us to explicitly reexpress the spatial average value of the Polyakov loop from Eq. (17) in terms of the reduced surface tension coefficients $\sigma_A(\beta)$.

6. Conclusions

In this work we have studied the phase transformation occurring in SU(2) gluodynamics using the clusters and anticlusters constructed from the Polyakov loops. At present the interest devoted to Polyakov loops clusters has been renewed and extended to full QCD with dynamical fermions, and some new aspects have been added [54] which make these clusters interesting for physics of heavy ion collisions. In order to investigate the anatomy of deconfining PT in a finite system we have applied the knowhow to describe clusters in the form of the liquid droplet model which is successfully used in theoretical studies of ordinary liquids, nuclear matter and spin systems. However, in contrast to these studies here we have analyzed a new type of objects, namely, the clusters formed by Polyakov loops of positive and negative signs. Also an important difference with previous applications of the liquid droplet

model is that we did not preset the value of Fisher exponent τ, but found its value from the requirement of best description of lattice data generated for all values of β studied here. This requirement has allowed us to determine the universal value of $\tau \simeq 1.806 \pm 0.008$ both for clusters and for anticlusters. This result is in contrast with the famous Fisher droplet model [8] which assumes $\tau > 2$, but is in line with the predictions of two exactly solvable statistical models with a tricritical endpoint [16, 20]. Our analysis has showed that the liquid droplet formula works well starting from dimers, only the monomers are not satisfactory described by it.

Our treatment shows that in the phase of unbroken $Z(2)$ symmetry among the SU(2) Polyakov loop clusters and anticlusters there are two large droplets of almost the same volume. According to the present framework they are considered as two different liquids. However, they are not homogeneous inside, but are filled by the smaller clusters which have the opposite sign of the Polyakov loops. Therefore, visually these liquids resemble two pieces of cheese of different sort.

These internal defects we have interpreted as a gas and applied to its description the liquid droplet model formula. Fit of the size distribution functions for the gas of clusters and the gas of anticlusters have allowed us to determine their reduced chemical potentials, surface tensions and overall normalization factors. As expected, in the symmetric phase the thermodynamic parameters of clusters and anticlusters are the same within error bars. The situation, however, drastically changes for $\beta > 2.5115$. The largest droplet (largest anticluster) increases in size and the total number of clusters inside it also increases, while the next largest droplet, which has an opposite sign of Polyakov loop, (largest cluster) shrinks and the number of anticlusters inside it also diminishes. Therefore, from the point of view of statistical mechanics it is correct to call these processes as condensation and evaporation, respectively. To our best knowledge this is the first simultaneous analysis of the collective properties of the two kinds of liquid droplets and their gases in SU(2) gluodynamics.

We have demonstrated that the deconfinement PT in SU(2) gluodynamics can be easily recognized by the different behavior of chemical potentials, surface tensions and overall normalization factors characterizing the two gases. Thus, the reduced surface tension of the gas of anticlusters increases with β, while the one of clusters gradually decreases and vanishes at $\beta > 3$. A similar behavior is found also for the corresponding chemical potentials. Hence, we conclude that above $\beta = \beta_c^\infty = 2.5115$, the two gases are not in a chemical equilibrium with each other. Our analysis shows that all studied thermodynamic quantities characterizing the Polyakov loop clusters have bifurcation point at $\beta = \beta_c^\infty$, i.e. their β derivatives on both sides of the point $\beta = \beta_c^\infty$ are not equal to each other. Here we did not study the thermodynamic limit of the system under investigation and, hence, we cannot determine an exact value of the (anti)cluster surface tension in physical units. Nevertheless, our approach is able to predict the functional behavior of the surface tension in physical units for the gas of clusters at high temperatures. It is $\sigma_{cl}^{phys}(T) \simeq T^2$. For anticlusters at high temperatures we found $\sigma_{acl}^{phys}(T) \simeq T^4$, but we believe that this function may include also an additional dependence on the reduced chemical potential μ_{acl}.

We have found an approximate relation between the spatial average of the Polyakov loop in terms of the difference between the volume of the largest anticluster $\max K_{acl}(\beta)$ and the volume of the largest cluster $\max K_{cl}(\beta)$. The investigation of the β-dependence of the two volumes $\max K_A(\beta)$ in the right hand side vicinity of the point $\beta = 2.52$ has allowed us to determine the exponents b_A, which within the error bars coincide with the critical exponent $\beta_{\rm Ising} = 0.3265 \pm 0.0001$ [52] of 3-dimensional Ising model and with the critical exponents $\beta_{\rm liquids} = 0.335 \pm 0.015$ [53] of simple liquids. Similarly, we determined the critical exponents

of the reduced surface tension coefficient $\sigma_A(\beta)$ in the right hand side vicinity of the point $\beta = 2.52$. This has allowed us to establish the scaling laws between $\sigma_A(\beta)$ and $\max K_{acl}(\beta)$, which help us to express the spatial average of the Polyakov loop in terms of the reduced surface tension coefficient σ_A of clusters and anticlusters. Thus, we explicitly show that the reduced surface tension coefficients σ_{cl} and σ_{acl} can be used as the order parameter of this PT.

Also we found an intriguing conservation law of volume fraction of auxiliary vacuum (see Fig. 1). In other words, for a given cut-off the volume fraction of vacuum is independent of β. This interesting phenomenon, however, requires further investigation.

In conclusion we want to stress that applying the LDM to the description of the (anti)clusters formed by the Polyakov loops gave us many interesting and unexpected results. In particular, the existing exactly solvable models of physical clusters should be further developed in order to be applicable for the SU(3) gluodynamics. Obviously, studies of clustering phenomena in the QCD PT should be continued within more realistic models including quark degrees of freedom.

Acknowledgements. Authors thank D. B. Blaschke, O. A. Borisenko, V. Chelnokov, Ch. Gattringer, D. H. Rischke, L. M. Satarov, H. Satz and E. Shuryak for the fruitful discussions and valuable comments. A.I.I., K.A.B., D.R.O., V.V.S., V.K.P. and G.M.Z. acknowledge a partial financial support of this work by the Program of Fundamental Research of the Department of Physics and Astronomy of National Academy of Sciences of Ukraine and by the National Academy of Sciences of Ukraine Grant of GRID simulations for high energy physics. I.N.M. acknowledges a partial support from the Helmholtz International Center for FAIR (Germany) and by the grant NSH-932.2014.2 of the Ministry of Education and Science of the Russian Federation.

References

[1] L. G. Yaffe and B. Svetitsky, Phys. Rev. D **26**, (1982) 963.

[2] L. G. Yaffe, and B. Svetitsky, Nucl. Phys. B **210**, (1982) 423.

[3] J. Polonyi and K. Szlachanyi, Phys. Lett. B **110**, (1982) 395.

[4] S. Fortunato and H. Satz, Phys. Lett. B **475**, (2000) 311.

[5] S. Fortunato *et. al.,* Phys. Lett. B **502**, (2001) 321.

[6] C. Gattringer, Phys. Lett. B **690**, (2010) 179.

[7] C. Gattringer and A. Schmidt, JHEP **1101** (2011) 051.

[8] M. E. Fisher, Physics **3**, (1967) 255.

[9] M. E. Fisher, Rep. Prog. Phys. **30**, (1969) 615.

[10] H. E. Stanley, Rev. Mod. Phys. **71**, (1999) S358.

[11] R. Guida and J. Zinn-Justin, J. Phys. Math. Gen. **31**, (1998) 8103.

[12] J. P. Bondorf, A. S. Botvina, A. S. Iljinov, I. N. Mishustin, K. Sneppen, Phys. Rep. **257**, 131 (1995).

[13] A. Dillmann and G. E. A. Meier, J. Chem. Phys. **94**, (1991) 3872.

[14] I. J. Ford, J. Chem. Phys. **106**, (1997) 9734.

[15] K. A. Bugaev, M. I. Gorenstein, I. N. Mishustin and W. Greiner, Phys. Rev. **62** (2000); Phys. Lett. B **498**, 144 (2001).

[16] P. T. Reuter, K. A. Bugaev, Phys. Let. B **517**, 233 (2001); Ukr. J. Phys. **52**, 489 (2007).

[17] J. I. Kapusta, Phys. Rev. D **23**, 2444 (1981).

[18] K. A. Bugaev, Phys. Rev. C **76** (2007) 014903; Phys. Atom. Nucl. **71**, 1615 (2008).

[19] K. A. Bugaev, V. K. Petrov and G. M. Zinovjev, Phys. Part. Nucl. Lett. **9**, 238 (2012).

[20] A. I. Ivanytskyi, Nucl. Phys. A **880**, 12 (2012); arXiv:1104.1900 [hep-ph].

[21] A. I. Ivanytskyi, K. A. Bugaev, A. S. Sorin and G. M. Zinovjev, Phys. Rev. E **86**, (2012) 061107.

[22] A. I. Ivanytskyi and K. A. Bugaev, Ukr. J. Phys. **57**, (2012) 964.

[23] see, for instance, F. Becattini, M. Bleicher, T. Kollegger, M. Mitrovski, T. Schuster and R. Stock, Phys.Rev. C85, (2012) 044921 and references therein.

[24] E. V. Shuryak, Prog. Part. Nucl. Phys. **62**, (2009) 48.

[25] K. A. Bugaev, Acta. Phys. Polon. B **36**, (2005) 3083.

[26] K. A. Bugaev, Phys. Part. Nucl. **38**, (2007) 447.

[27] J. Borg, I. N. Mishustin and J. P. Bondorf, Phys. Lett. B **470** (1999) 13.

[28] L. G. Moretto *et al.*, Phys. Rev. C **68**, (2003) 1602, and references therein.

[29] L. G. Moretto *et al.*, Phys. Rev. Lett. **94**, (2005) 202701 and references therein.

[30] V. V. Sagun, A. I. Ivanytskyi, K. A. Bugaev and I. N. Mishustin, Nucl. Phys. A **924**, (2014) 24.

[31] T. L. Hill, *Thermodynamics of small systems*, New York: Dover, 1994.

[32] L. G. Moretto *et al.*, Phys. Rep. **287**, 249 (1997).

[33] D. H. E. Gross, *Microcanonical Thermodynamics: Phase Transitions in Finite Systems*, Lecture Notes in Physics, **66**, Singapor: World Scientific, 2001.

[34] Ph. Chomaz, F. Gulminelli and V. Duflot, Phys. Rev. E. **64** (2001) 046114.

[35] O. Lopez and M. F. Rivet, Eur. Phys. J. A. **30**, (2006) 263 and references therein.

[36] M. I. Polikarpov, Phys. Usp. **38**, (1995) 591.

[37] J. R. Taylor, *"An introduction to error analysis", University Science Book Mill Valley, California (1982).*

[38] J. Fingberg, U. Heller and F. Karsch, Nucl. Phys. B **392**, (1993) 493.

[39] C. Gattringer and C. Lang, *"Quantum Chromodynamics on the Lattice"*, Springer, Berlin, 2010.

[40] F. Karsch and E. Laermann, In Hwa, R.C. (ed.) et al.: *"Quark gluon plasma"* (2003) 1; [hep-lat/0305025].

[41] E. Farhi and R. L. Jaffe, Phys. Rev. D **30**, (1984) 2379.

[42] I. Mardor and B. Svetitsky , Phys. Rev. D **44**, (1991) 878.

[43] G. Neergaard and J. Madsen, Phys. Rev. D **62** (2000) 034005.

[44] L. F. Palhares and E. S. Fraga, Phys. Rev. D **82**, (2010) 125018.

[45] M. B. Pinto, V. Koch and J. Randrup, Phys. Rev. C **86**, (2012) 025203.

[46] D. N. Voskresensky, M. Yasuhira, and T. Tatsumi, Nucl. Phys. A723, 291 (2003).

[47] K. A. Bugaev and G. M. Zinovjev, Nucl. Phys. A **848**, (2010), 443.

[48] M. G. Alford, K. Rajagopal, S. Reddy, and F. Wilczek, Phys. Rev. D **64**, (2001) 074017.

[49] G. Endrodi, C. Gattringer and H.-P. Schadler, Phys. Rev. D **89**, (2014) 054509.

[50] I. Zakout, C. Greiner, and J. Schaffner-Bielich, Nucl. Phys. A 781, (2007) 150.

[51] I. Zakout and C. Greiner, Phys. Rev. C 78, (2008) 034916.

[52] M. Campostrini, A. Pelissetto, P. Rossi and E. Vicari, Phys. Rev. E **65**, (2002) 066127.

[53] K. Huang, *Statistical Mechanics*, Wiley, New York, 1987.

[54] A. Schäfer, G. Endrodi and J. Wellnhofer, Phys. Rev. D **92**, (2015) 014509.

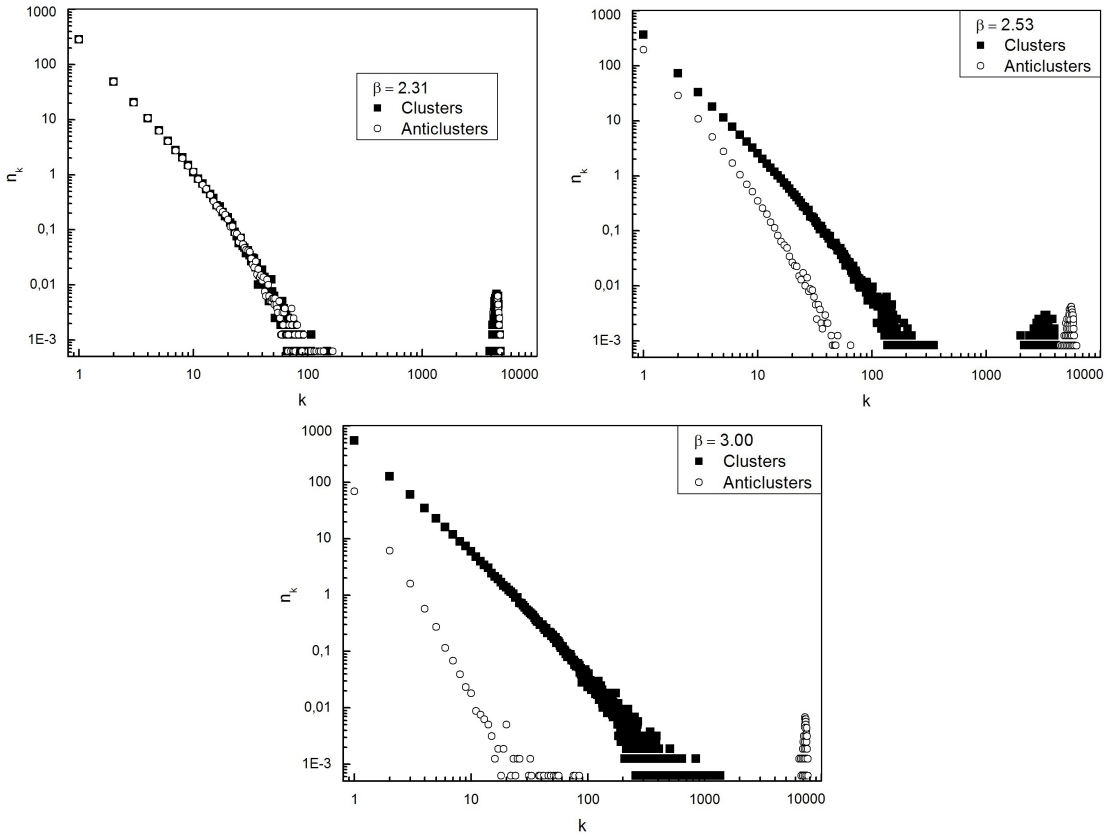

Figure 2: Ensemble average size distributions of clusters (squares) and anticlusters (circles) for different β values. k is the size of an (anti)cluster, n_k is its multiplicity. **Upper left panel:** For $\beta < \beta_c^\infty$ ($\beta_c^\infty = 2.5115$ is the deconfinement point for $N_\tau = 8$ in the gauge system) one can see a complete symmetry between the two distributions. The largest (anti)cluster is of the mean size $k \simeq 4500$, which is well separated from the distribution of the corresponding gas of smaller (anti)clusters. **Upper right panel:** Same as in the upper left panel, but for $\beta = 2.53$ which is slightly above β_c^∞. One can see now an emerging difference between the two distributions: the multiplicities in the gas of clusters are higher than the multiplicities in the gas of anticlusters, whereas the largest anticluster is noticeably larger than the largest cluster. **Lower panel:** Same as in upper panels, but for $\beta = 3.0$, which is well above β_c^∞. The largest cluster is now inseparable from the corresponding cluster gas. The statistical errors are of the order of the size of symbols or smaller. All these results refer to a cut-off $L_{cut} = 0.2$.

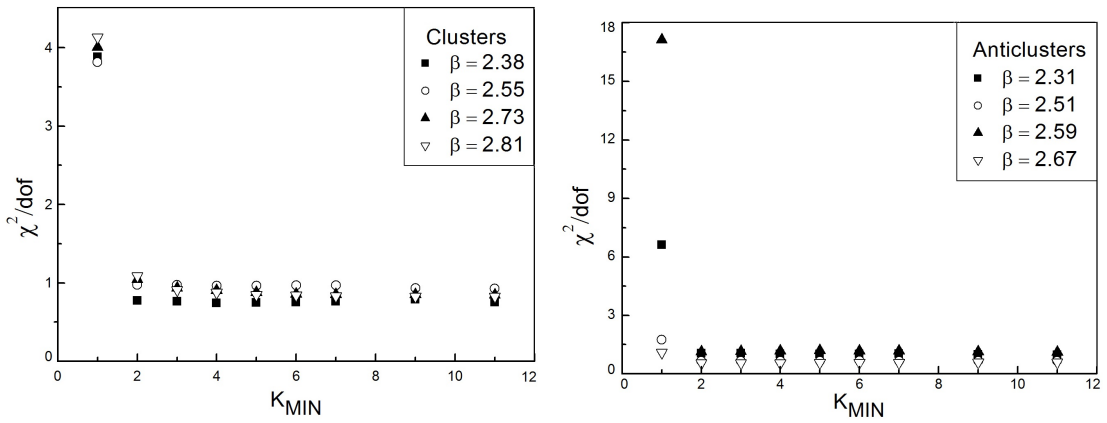

Figure 3: χ^2/dof results of the 4-parametric fit by the LDM formula for different k_{min} are shown for a few selected values of β: left for clusters, right for anticlusters. As one can see from both panels, only the monomers are not described by the LDM formula. Results are shown for $L_{cut} = 0.2$.

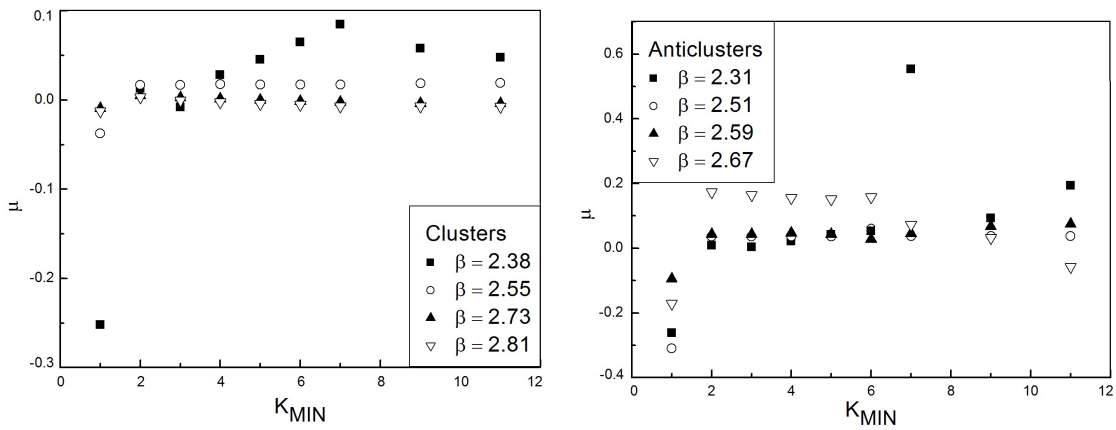

Figure 4: Values of the reduced chemical potentials μ_A, found from 4-parametric fitting of the LDM formula, are shown for several values of k_{min} and for a few values of β. Similar results are found for other values of β. All these results refer to the choice of cut-off $L_{cut} = 0.2$.

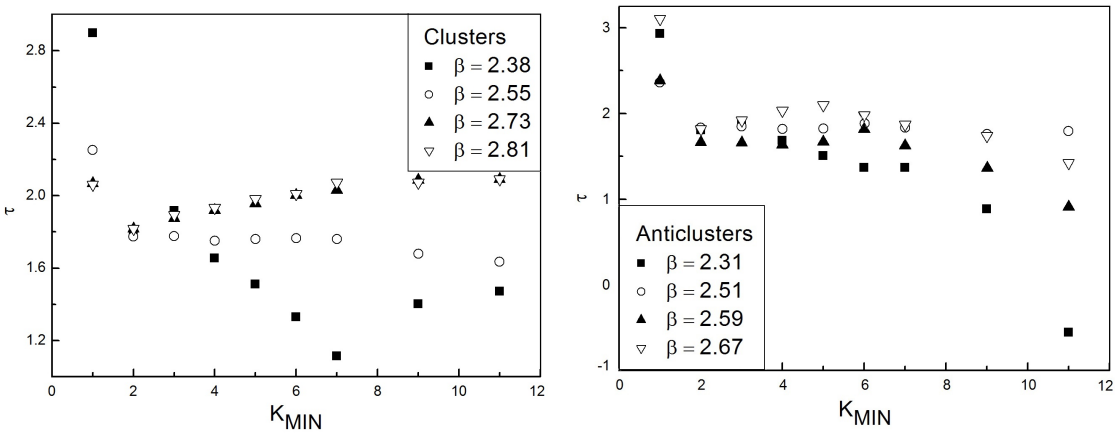

Figure 5: The Fisher exponent τ for several values of k_{min} and for a few values of β found by the 4-parametric fitting of the LDM formula. Similar results are found for other values of β. All these results refer to a cut-off $L_{cut} = 0.2$.

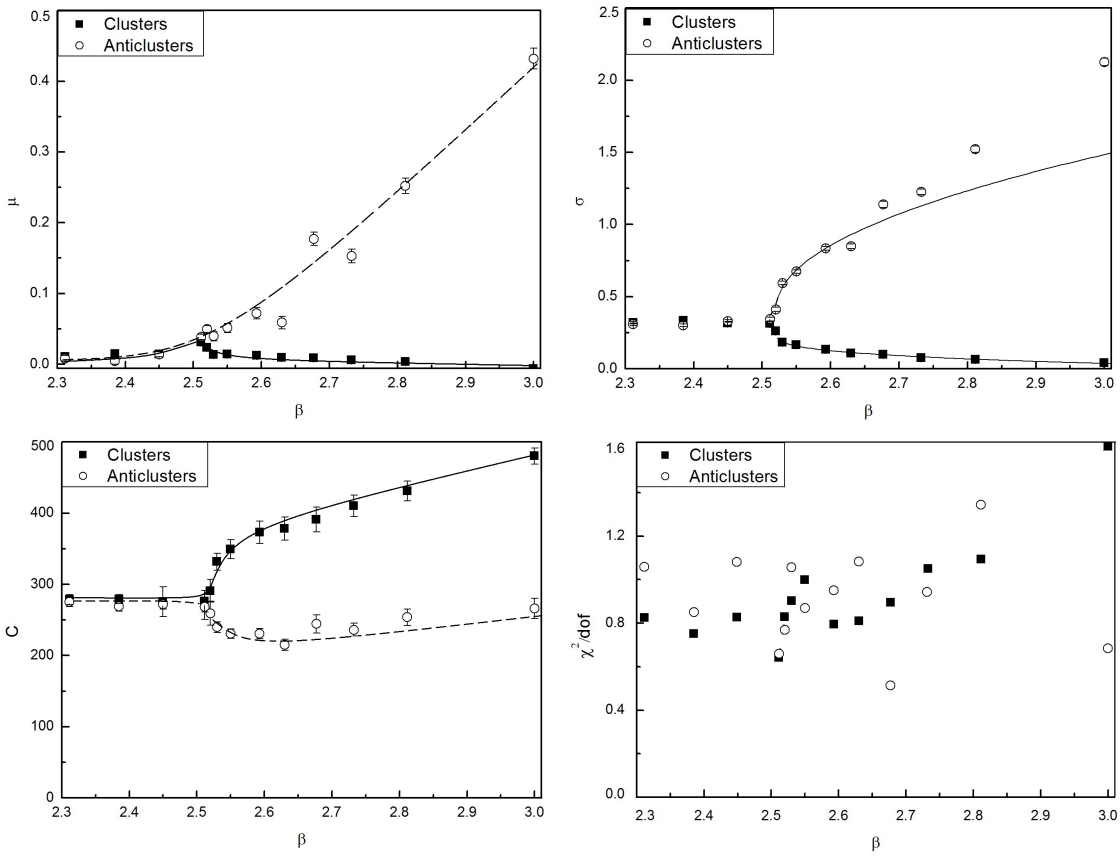

Figure 6: Results of the 3-parametric fit for the β-dependence of the reduced chemical potential μ_A, of the reduced surface tension σ_A, of the normalization constant C_A and of the mean deviation squared per degree of freedom χ^2/dof. The fit parameters are shown for $k_{min} = 2$ at fixed $\tau_A = 1.806 \pm 0.008$ for the data obtained for cut-off $L_{cut} = 0.2$. In the panels depicting μ_A and C_A the curves are shown to guide the eye, while in the panel of σ_A the curves represent Eq. (20). More details are given in the text.

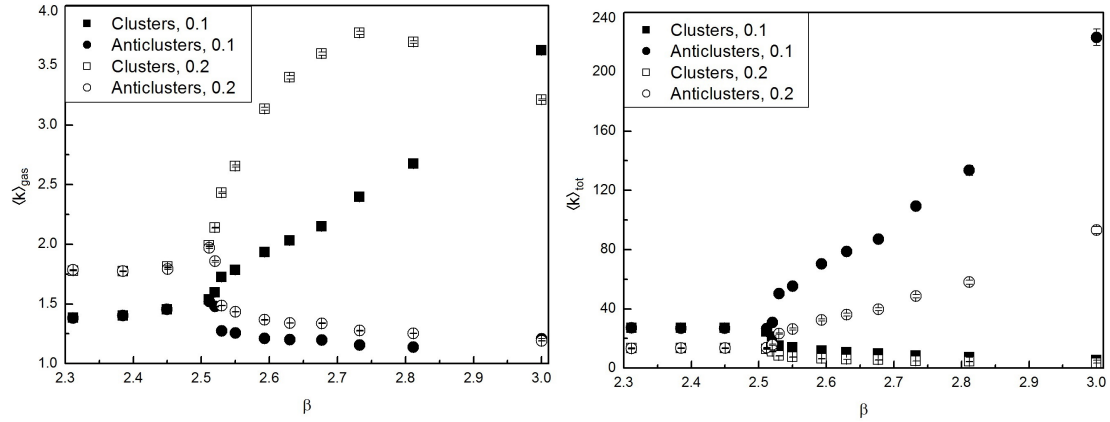

Figure 7: The β-dependence of the mean cluster volume $\langle k_A \rangle_{gas}$ in the A-gas (left) and the mean total cluster volume $\langle k_A \rangle_{tot}$ including the A-gas and the A-liquid droplet (right). Results are shown for $L_{cut} = 0.1$ and $L_{cut} = 0.2$.

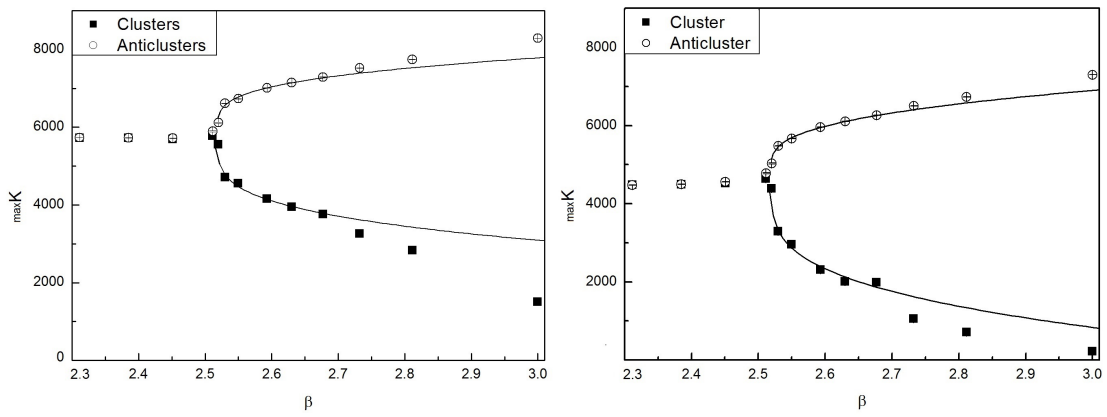

Figure 8: The β-dependence of the volume of the largest anticluster and the largest cluster. Results are shown for $L_{cut} = 0.1$ (left) and $L_{cut} = 0.2$ (right). The curves represent Eq. (19). More details are given in the text.

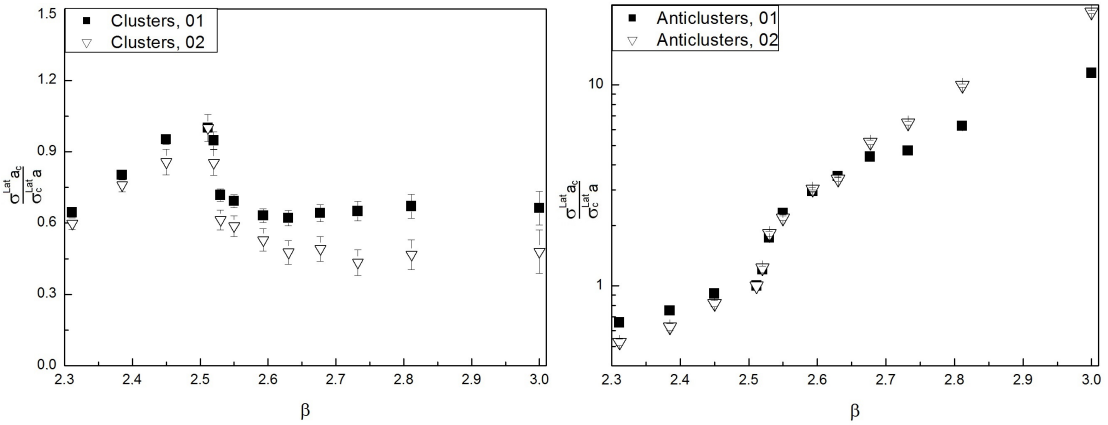

Figure 9: The β-dependence of the lattice surface tension in relative units $\frac{\sigma_A(\beta)\, a_\sigma(\beta_c^\infty)}{\sigma_A(\beta_c^\infty)\, a_\sigma(\beta)}$ is shown for clusters (left) and anticlusters (right) for two cut-off values $L_{cut} = 0.1$ and $L_{cut} = 0.2$.

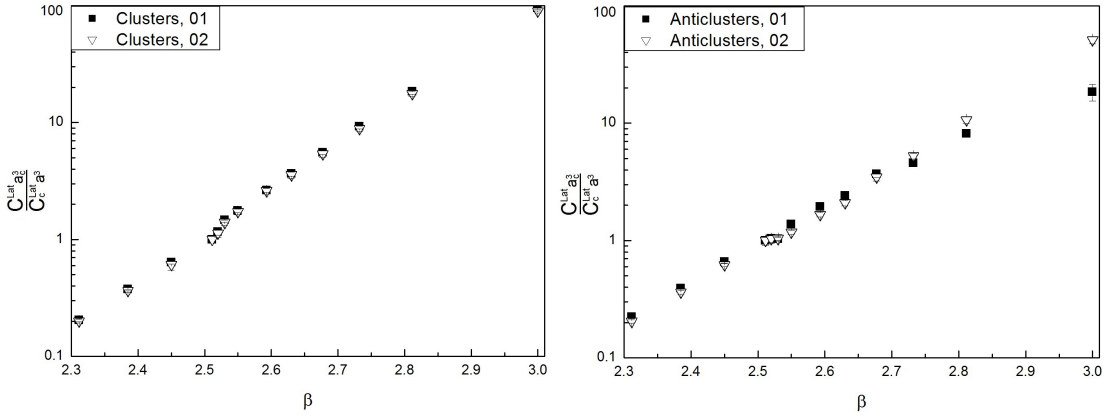

Figure 10: Same as in Fig. 9, but for the normalization factors in physical units $\frac{C_A^{phys}(\beta)}{C_A^{phys}(\beta_c^\infty)}$ according to Eq. (8).

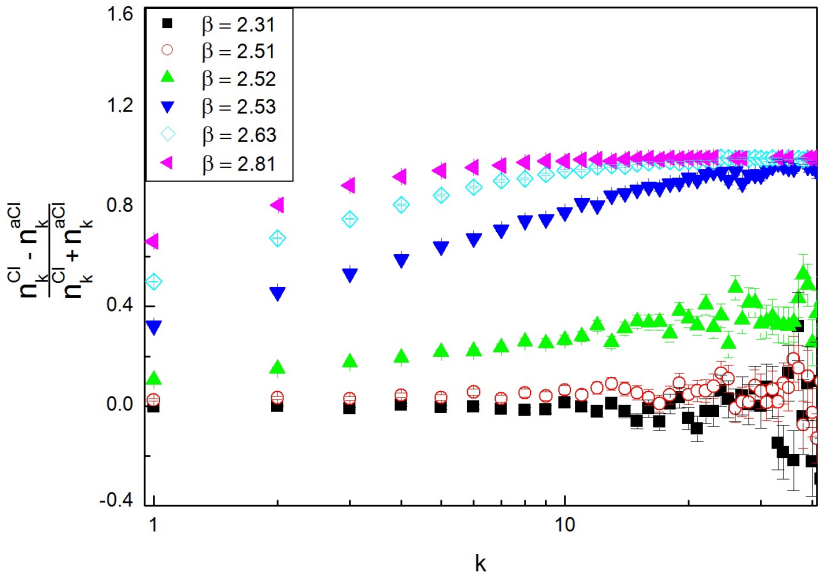

Figure 11: (Color online) The relative asymmetry $\frac{n_{cl}(k)-n_{acl}(k)}{n_{acl}(k)+n_{cl}(k)}$ of the cluster-anticluster multiplicity as function of the (anti)cluster volume k is shown for several values of β. All results correspond to the cut-off $L_{cut} = 0.2$.